Please cite this article in press as: Klenow et al., Shape of the membrane neck around a hole during plasma membrane repair, Biophysical Journal (2024), https://doi.org/10.1016/j.bpj.2024.05.027

Biophysical Journal
Article

Biophysical Society

Shape of the membrane neck around a hole during plasma membrane repair

Martin Berg Klenow,[1] Magnus Staal Vigsø,[1] Weria Pezeshkian,[2] Jesper Nylandsted,[3,4] Michael Andersen Lomholt,[1] and Adam Cohen Simonsen[1,*]

[1]PhyLife - Physical LifeScience, Department of Physics Chemistry and Pharmacy, University of Southern Denmark (SDU), Campusvej 55, Odense M, Denmark; [2]Niels Bohr Institute, University of Copenhagen, Copenhagen, Denmark; [3]Danish Cancer Institute (DCI), Copenhagen Ø, Denmark; and [4]Department of Molecular Medicine, University of Southern Denmark, Odense C, Denmark

ABSTRACT Plasma membrane damage and rupture occurs frequently in cells, and holes must be sealed rapidly to ensure homeostasis and cell survival. The membrane repair machinery is known to involve recruitment of curvature-inducing annexin proteins, but the connection between membrane remodeling and hole closure is poorly described. The induction of curvature by repair proteins leads to the possible formation of a membrane neck around the hole as a key intermediate structure before sealing. We formulate a theoretical model of equilibrium neck shapes to examine the potential connection to a repair mechanism. Using variational calculus, the shape equations for the membrane near a hole are formulated and solved numerically. The system is described under a condition of fixed area, and a shooting approach is applied to fulfill the boundary conditions at the free membrane edge. A state diagram of neck shapes is produced describing the variation in neck morphology with respect to the membrane area. Two distinct types of necks are predicted, one with conformations curved beyond π existing at positive excess area, whereas flat neck conformations (curved below π) have negative excess area. The results indicate that in cells, the supply of additional membrane area and a change in edge tension is linked to the formation of narrow and curved necks. Such necks may be susceptible to passive or actively induced membrane fission as a possible mechanism for hole sealing during membrane repair in cells.

SIGNIFICANCE Rupture of cellular plasma membranes compromise homeostasis, and holes must be sealed rapidly to prevent cell death. A mechanistic understanding of plasma membrane repair is critical for a fundamental understanding of membrane remodeling and for developing therapeutic strategies that target repair in, e.g., cancer cells. The membrane repair machinery is diverse but involves recruitment of annexin proteins, known to induce membrane curvature, and the supply of extra membrane area near the hole. We establish a theoretical model for the membrane shape around a hole that is solved numerically. The model yields a state diagram of neck conformations and provides a basis for identifying membrane conformations with potential relevance in a repair mechanism.

INTRODUCTION

Membranes of eukaryotic cells play fundamental roles in compartmentalizing the cell interior and as a boundary to the exterior. Unlike prokaryotic cells, which are shielded by a cell wall, mammalian cells are protected by their plasma membrane and are susceptible to membrane injury during the cellular life-cycle (1). Disruption of the plasma membrane integrity poses an immediate threat, and holes must be sealed rapidly to ensure cell survival. Eukaryotes have evolved a robust membrane repair machinery comprising the recruitment of multiple repair proteins to the damage site as triggered by the influx of calcium ions (2–4). The mechanisms of membrane repair are incompletely understood and a matter of significant interest, not least because diseases including several cancer types and muscular dystrophy are associated with abnormal function of the membrane repair machinery. A deeper mechanistic understanding of membrane repair would aid the development of future therapies that target the repair process (5). The annexin family of cytosolic proteins comprises key players in membrane repair by locating to the damage site and facilitating remodeling of the plasma membrane (6–8). The twelve annexins in mammals (ANXA1–ANXA11 and ANXA13) share a conserved core

Submitted November 12, 2023, and accepted for publication May 28, 2024.

*Correspondence: adam@sdu.dk

Editor: Michael Kozlov.

https://doi.org/10.1016/j.bpj.2024.05.027

Please cite this article in press as: Klenow et al., Shape of the membrane neck around a hole during plasma membrane repair, Biophysical Journal (2024), https://doi.org/10.1016/j.bpj.2024.05.027

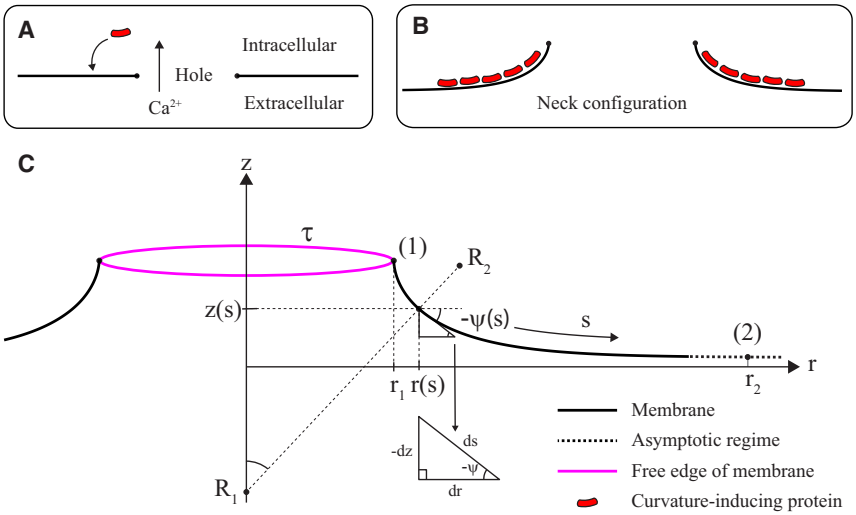

FIGURE 1 Schematic illustration of definitions in the axisymmetric model for membrane curvature near a hole during plasma membrane repair. After membrane damage, Ca^{2+} ions enter the cell and activate curvature-inducing proteins binding to the intracellular membrane leaflet and inducing a spontaneous curvature c_0 (*A and B*). The membrane shape is described by the height $z(s)$, radius $r(s)$, and angle $\psi(s)$ as a function of the arc length s (*C*). A free membrane edge with line tension τ exists at the hole border. To obtain the shape parameters under stationary conditions, variational calculus is performed on the total energy functional. The shape equations with boundary terms are subsequently solved numerically. For further definitions, see the text. To see this figure in color, go online.

domain at the C-terminus that binds to negatively charged membrane lipids in the presence of Ca^{2+}. The membrane-binding face of the core domain is convexly shaped and was shown in simulations to induce negative membrane curvature upon binding (9) and in experiments to bind membranes with a curvature sensitive affinity (10). Annexin-induced membrane curvature was demonstrated in planar membrane patches with free edges, mimicking the membrane structure near a hole (11,12). Notably, ANXA4, ANXA5, and other family members generated roll-up of the membrane patch within seconds, as initiated from the free edges. Rolling provides evidence for the curvature-inducing capacity of annexins and points to a mechanistic role of membrane bending during repair. Despite the evidence for membrane curvature induced by annexins in membrane model systems, it is not fully understood how curvature near a hole may assist sealing of the membrane. In this context, theoretical and computational modeling are important tools due to the challenges of observing short-lived membrane conformation near pores in experiments. We previously proposed (11) that spontaneous curvature promoted by annexin binding to the intracellular leaflet induces the formation of a curved neck around a hole, as illustrated in Fig. 1 *B*. Indeed, the accumulation of multiple annexins after rupture points to curvature as a key element of the repair mechanism. Here, we focus on a simplified description of the stationary membrane morphologies that can exist near a hole. Such conformations may represent potential transition states to the final sealed membrane, possibly involving the action of additional repair proteins interacting with the transition state conformation to promote sealing. When defining a model for the membrane shape around a hole, one must specify constraints and in particular whether the membrane is equilibrated under a condition of constant membrane tension or under constant membrane area. In a free-standing lipid bilayer without spontaneous curvature (e.g., in giant vesicles (GUVs) without proteins), an assumption of constant membrane tension is typically considered relevant (13), in which case a membrane hole is inherently unstable against expansion or contraction. However, in cells, the presence of immobile transmembrane proteins has been shown to resist membrane flow and to result in a slow relaxation of tension variations over timescales of tens of minutes (14,15). Based on this, a constant tension approximation is unlikely to describe the plasma membrane within the short timescale (tens of seconds) of membrane repair (16). Alternatively, by assuming that on the timescale of repair and in the local membrane region around the rupture, the membrane is equilibrated to a fixed membrane area, the tension will be set by the size of the hole. In the latter ensemble, transiently stable membrane conformations around a hole can exist. In partial support of this picture, we note that during plasma membrane repair, the cortical actin is depolymerized and remodeled in a local neighborhood around the membrane rupture (17). Decoupling from the cytoskeleton may create a local region of semi-free membrane near the hole and may provide, within the timescale of repair, a condition of constant area. Although our model includes a constant area constraint, further studies in cells are required to fully corroborate the assumptions of this description. The membrane curvature elastic energy can be described by the Helfrich expression (18), and minimization of the total energy using variational calculus follows the procedure outlined by Seifert et al. (19–21) and used in multiple studies to obtain the equilibrium conformation of membrane systems subject to boundary conditions. Examples of this procedure include models of membrane budding in endo- and exocytosis induced by the binding of curvature-inducing proteins (22–24), wrapping of membranes around nanoparticles (25), and modeling of lipid lenses and droplets in bilayers and the spontaneous budding of lipid droplets from bilayers (26,27). Other examples are the formation of neck structures induced by leaflet

Please cite this article in press as: Klenow et al., Shape of the membrane neck around a hole during plasma membrane repair, Biophysical Journal (2024), https://doi.org/10.1016/j.bpj.2024.05.027

asymmetry through binding of curvature-inducing molecules. Such systems may be further complicated by a spatial variation in the spontaneous curvature that equilibrates with the neck shape (28,29). Studies of the conformation of free-edged membranes subject to spontaneous curvature are mostly limited to vesicle rupture by pore formation (30–35). Our model for the membrane shape near a hole takes into account spontaneous curvature, line tension at the free edge, and imposing a fixed membrane area. In this representation, the membrane tension is set by the condition of constant area. The membrane area is referenced against a flat intact membrane such that the difference (the "excess area") can be used to classify the shape solutions. Negative excess area implies that the membrane lacks the necessary area to seal a hole, whereas a positive excess area implies that a sufficient area for sealing the hole is available. We construct a state diagram for membrane neck conformations in order to explore the conditions with potential relevance for membrane repair. The model describes how the excess area and the line tension at the free edge regulate the neck geometry. The results indicate that in cells, the supply of additional membrane area after rupture is required for the formation of curved neck conformations around the hole with potential relevance for a repair mechanism.

MATERIALS AND METHODS

Formulation of a model for the neck shape

The shape of a membrane near a hole is modeled under the assumption of axial symmetry and the model is explained in detail in the supporting material. Briefly, the model uses the Helfrich description for the membrane curvature elastic energy (18) and additionally takes into account the line tension at the free membrane edge and the tension in the membrane plane. Referring to Fig. 1 *C*, the membrane near the free edge of the hole (marked state (1)) is curved, whereas it approaches a planar conformation in the asymptotic limit of large radii away from the hole. Curvature is generated by the binding of repair proteins to the cytosolic side of the membrane and modeled by a spontaneous curvature term (c_0) in the Helfrich Hamiltonian. In the absence of membrane tension, the free energy of the membrane neck is the sum of the Helfrich curvature elastic energy plus a contribution from line tension τ at the free membrane edge:

$$G_{\text{neck}} = \int_A \left[\frac{k}{2}(2H - c_0)^2 + k_G K\right] dA + 2\pi\tau r_1 \quad \text{(Equation 1)}$$

Here k is the "mean curvature modulus," k_G is the "Gaussian curvature modulus," and the area integration is over a sufficiently large area A near the hole to obtain convergence to an asymptotic analytical solution. The total curvature $2H$ and the Gaussian curvature K are related to the principal curvature radii R_1, R_2 via

$$2H = \frac{1}{R_1} + \frac{1}{R_2} \quad \text{(Equation 2)}$$

$$K = \frac{1}{R_1 R_2} \quad \text{(Equation 3)}$$

The shape coordinates $r(s)$, $z(s)$, and $\psi(s)$ are parameterized in terms of the arc length s running along the membrane surface in the radial direction. The tension energy is included with the term

$$G_{\text{tension}} = \sigma(A - A_0) = 2\pi \int_{s_1}^{s_2} \sigma r ds - \sigma A_0, \quad \text{(Equation 4)}$$

where σ can be interpreted as a membrane tension, A is the membrane area, and A_0 the area in a reference state. Energy minimization using variational calculus is performed under the constraint of constant membrane area, in which case the tension parameter σ in Eq. (4) is set by the condition of constant area. The definition of tension follows previous work (36). Importantly, it must also be noted that to obtain the so-called total (or effective) membrane tension σ_{tot}, one needs to add a spontaneous tension term originating from spontaneous curvature (37): $\sigma_{\text{tot}} = \sigma + \frac{1}{2}kc_0^2$. In the case of zero spontaneous curvature, one gets $\sigma_{\text{tot}} = \sigma$. Since neck formation around holes is driven by a nonzero spontaneous curvature, it is important to distinguish between the tension parameter σ in the model and the total membrane tension as can be measured experimentally (38,39). The equilibrium neck conformation is established by requiring the variation to vanish: $\delta S = 0$, where the total energy functional S is given as

$$S = \frac{G_{\text{neck}} + G_{\text{tension}}}{2\pi} = \int_{s_1}^{s_2} \mathcal{L}\, ds - k_G \cos\psi\big|_{s_1}^{s_2} + \tau r_1, \quad \text{(Equation 5)}$$

with the "Lagrangian" $\mathcal{L}$:

$$\mathcal{L} = \frac{k}{2}\left(\dot{\psi} + \frac{\sin\psi}{r} - c_0\right)^2 r + t(\dot{r} - \cos\psi) + v(\dot{z} - \sin\psi) + \sigma r \quad \text{(Equation 6)}$$

The functions $v = v(s)$ and $t = t(s)$ are Lagrange multipliers related to geometrical constraints. Application of the variational principle yields a set of Euler-Lagrange type equations, which reduce to the following coupled shape equations (for details see supporting material):

$$\dot{\tilde{r}} = \cos\psi \quad \text{(Equation 7)}$$

$$\dot{\tilde{\psi}} = \tilde{u} \quad \text{(Equation 8)}$$

$$\dot{\tilde{u}} = -\tilde{u}\frac{\cos\psi}{\tilde{r}} + \frac{\sin\psi\cos\psi}{\tilde{r}^2} + \tilde{t}\frac{\sin\psi}{k\tilde{r}} \quad \text{(Equation 9)}$$

$$\dot{\tilde{t}} = \frac{1}{2}\left[(\dot{\psi} - 1)^2 - \frac{\sin^2\psi}{\tilde{r}^2}\right] + \tilde{\sigma} \quad \text{(Equation 10)}$$

$$\dot{\tilde{z}} = \sin\psi \quad \text{(Equation 11)}$$

$$\dot{\tilde{A}} = 2\pi\tilde{r} \quad \text{(Equation 12)}$$

Here, we have applied dimensionless variables that eliminate the explicit dependence on c_0 and k and make it simpler to map out the neck configurations near a hole because of a lower number of variables. The dimensionless variables (denoted with $\sim$) are: $\tilde{s} = s/l_c$, $\tilde{r} = r/l_c$, $\tilde{z} = z/l_c$, $\tilde{t} = t/\tau_c$, $\tilde{\tau} = \tau/\tau_c$, $\tilde{\sigma} = \sigma/\sigma_c$, $\tilde{A} = A/l_c^2$, and $\tilde{S} = S/k$, using the following characteristic quantities:

Please cite this article in press as: Klenow et al., Shape of the membrane neck around a hole during plasma membrane repair, Biophysical Journal (2024), https://doi.org/10.1016/j.bpj.2024.05.027

Characteristic length scale: $l_c = \frac{1}{c_0}$
Characteristic tension: $\sigma_c = kc_0^2$
Characteristic line tension: $\tau_c = kc_0$

In dimensionless units, the total membrane tension becomes $\tilde{\sigma}_{\text{tot}} = \tilde{\sigma} + \frac{1}{2}$. The variational calculus also produces two boundary conditions that must be fulfilled at the free edge:

$$\frac{k_G}{k} = (1 - \dot{\psi}_1)\frac{\tilde{r}_1}{\sin\psi_1} - 1 = \alpha \qquad \text{(Equation 13)}$$

$$\tilde{t}(\tilde{s}_1) = \tilde{t}_1 = \tilde{\tau} \qquad \text{(Equation 14)}$$

Numeric solutions to the shape equations

The shape equations in dimensionless units are solved numerically in MATLAB. Generating numeric solutions presents two challenges: 1) we need an initial state for the numeric integration, and 2) the boundary conditions in Eqs. (13) and (14) must be fulfilled at the free edge. For addressing 1), we solve analytically the equations to first order in the nearly planar regime with a flat asymptotic limit of the neck profile far away from the hole. We use this solution to generate a physically valid initial state for integration finitely far away from the hole. To fulfill the boundary conditions at the free edge, 2) we apply a "shooting" approach to identify the solutions of the shape equations that fulfill the boundary conditions. Shooting is performed by varying the angle ψ_2 over a wide range to search the solution space. Physically valid solutions are those that match both boundary conditions in Eqs. (13) and (14).

The shape equations are formulated under a condition of constant area, which in turn determine the membrane tension. But for computational reasons, the value of the membrane area cannot be specified in the initial state since a shooting approach is used for generating solutions. Instead, to map solutions with different membrane areas, the value of the tension $\tilde{\sigma}$ is varied, and the resulting solutions are sorted according to their areas. However, this does not change the underlying fact that the model is formulated using a constant area constraint. The membrane area $\tilde{A}_{\text{neck}}$ within the radius $\tilde{r}_2$ depends on the choice of the radius, and to eliminate this dependency, we use as a reference the area of a flat disk: $\tilde{A}_{\text{disk}} = \pi\tilde{r}_2^2$. The excess area defined as $\Delta\tilde{A} = \tilde{A}_{\text{neck}} - \tilde{A}_{\text{disk}}$ is used to classify solutions independently of $\tilde{r}_2$. For negative excess areas ($\Delta\tilde{A} < 0$), the membrane lacks sufficient area to seal a hole, whereas for positive values ($\Delta\tilde{A} > 0$), an excess area for repair is available. Likewise, the membrane energy $\tilde{S}$ will depend on the area, which in turn varies among solutions to the shape equations. In order to better compare energies of neck shapes with different areas, a reference state for the energy is chosen as the energy of a flat membrane with the same area as the curved state. Thus, the relative energy is $\Delta\tilde{S} = \tilde{S}_{\text{neck}} - \tilde{S}_{\text{flat}}$. The contribution to both $\Delta\tilde{A}$ and $\Delta\tilde{S}$ outside $\tilde{r}_2$ decays exponentially to zero when $\tilde{r}_2 \gg \lambda$.

Magnitude of physical parameters

It is relevant to consider realistic estimates of the bending modulus and the spontaneous curvature as used for constructing the characteristic membrane and line tensions in the model. The bending modulus of plasma membranes has been estimated by fluctuation analysis of giant plasma membrane vesicles to close to $k = 20k_BT = 8\cdot10^{-20}\,J$ at $37^\circ C$ (40). The mean curvature induced by single annexin A5 trimers binding to a membrane was found in MD simulations to be $0.032\ \text{nm}^{-1}$ (41). Recent MD simulations of the large scale membrane curvature generated by 2D packing of multiple annexins A5 trimers on a membrane, found a total curvature close to $0.025\ \text{nm}^{-1}$ or a curvature radius of 40 nm (42). The combined effect of multiple trimers provides a more realistic estimate of the spontaneous curvature generated by annexins during plasma membrane repair. Using the above numbers, we obtain the following characteristic quantities: $l_c = \frac{1}{c_0} = 40$ nm, $\sigma_c = kc_0^2 = 5\cdot10^{-5}\,\text{J/m}^2$, and $\tau_c = kc_0 = 2$ pN. The line tension of a free membrane edge has been measured using tension-induced rupture of GUVs with values generally in the range of 5–25 pN (13.43,44) with higher values typically measured for higher content of cholesterol in the membrane. This translates to values of the dimensionless line tension in the range of 2–10. The presence of detergent (Tween 20) decreases the line tension to around 0.2 pN (43). The characteristic membrane tension of $\sim 5\cdot10^{-5}\,\text{J/m}^2$ is smaller than the tensions of $\sim 10^{-3}\,\text{J/m}^2$ needed to increase the area per molecule but slightly larger than the tension ($\sim 10^{-6}\,\text{J/m}^2$) needed for stretching out thermal undulations in bilayers (45). In cellular systems, membrane tensions of the order $\sim 10^{-5}\,\text{J/m}^2$ have been measured in M2 macrophages (46) and values of the order $\sim 10^{-6}\,\text{J/m}^2$ in fibroblast cells (47) and MCF7 cells (48).

RESULTS

First, we illustrate the generation of numerical solutions to the shape Eqs. (7–12) to produce physical neck profiles around a hole. Fig. 2 shows the identification of two neck profiles that have a line tension of $\tilde{\tau} = 1$, a membrane tension of $\tilde{\sigma} = -0.1$, and excess areas $\Delta\tilde{A} = -1.8$ and 10.5, respectively. Due to the open membrane geometry at the free edge, a "shooting" approach is needed to identify the solutions that satisfy the boundary conditions at the free edge in Eqs. (13) and (14). Fig. 2 *A* shows that fulfillment of Eq. (14) by the Lagrange multiplier $\tilde{t}$ happens at the points (a–f) for two specific start angles (blue and red curves). When multiple initial angles are searched (shooting) as displayed in Fig. 2 *B*, it is found that Eq. (13) can only be fulfilled for the solutions marked at points (d,f). Now since only points (d,f) satisfy "both" of the two required boundary conditions at the free edge, the neck profiles corresponding to these points are the only physical solutions to the shape equations. No other solutions where found after an exhaustive search of the solution space using eight orders of magnitude variation in ψ_2 and integration beyond the point of membrane self-intersection. The two neck profiles identified by the shooting method in Fig. 2 *A* and *B* are plotted in Fig. 2 *C* and are also shown as 3D surfaces in Fig. 2 *D* and *E*. It is immediately clear that the two profiles have significantly different membrane angles at the free edge. The red profile with the lowest edge angle in Figs. 2, *C* and *D* ("flat neck") also has a negative excess membrane area, meaning that it lacks sufficient area for repair. In contrast, the blue neck profile with a larger edge angle ("curved neck") in Figs. 2, *C* and *E* has a positive excess area and therefore sufficient membrane area for repair. In general, the model consistently produces these two types of physical solutions (flat and curved necks) over a wide range of realistic parameter values. All solutions have zero variation in the total energy ($dS = 0$) as required for stable solutions. But we are not guaranteed that the solutions are not metastable/unstable (see also discussion). To obtain more insight into the variation of neck shapes, a series of neck profiles were calculated for

Please cite this article in press as: Klenow et al., Shape of the membrane neck around a hole during plasma membrane repair, Biophysical Journal (2024), https://doi.org/10.1016/j.bpj.2024.05.027

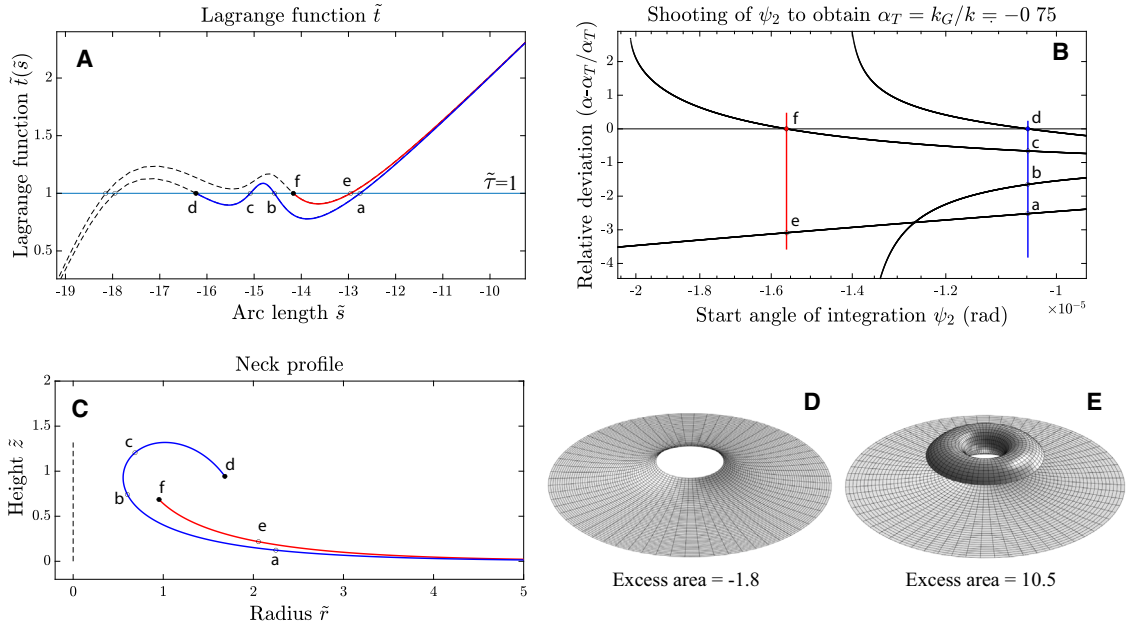

FIGURE 2 Examples of membrane neck shapes obtained by numerically solving the shape equations with $\tilde{\tau} = 1$ and $\tilde{\sigma} = -0.1$. A shooting procedure is employed to fulfill both the condition on the line tension given by Eq. (14) (*A*) and to fulfill the condition on the mechanical moduli by Eq. (13) (*B*). Searching (shooting) for these solutions is done by varying the membrane angle ψ_2 away from the hole. In the example, only the two points (d,f) in (*A*) and (*B*) fulfill both conditions. The corresponding two membrane neck shapes are shown in (*C*) and display a flat and curved neck geometry respectively. The neck shapes are also shown as 3D surfaces in (*D*) and (*E*). To see this figure in color, go online.

variations in the membrane tension $\tilde{\sigma}$ between -0.2 and 0.2 in Fig. 3 *A*. Note that the total membrane tension is defined as $\tilde{\sigma}_{\text{tot}} = \tilde{\sigma} + \frac{1}{2}$ and is positive for all configurations since $\tilde{\sigma} > -1/2$. The excess area is the difference between the neck area and the area of the projected flat disk without a hole, as illustrated in Fig. 3 *C*. For a fixed line tension $\tilde{\tau} = 1$, the solutions split up into curved and flat neck profiles, which can be separated using the cutoff $|\psi_1| = \pi$. The flat necks consistently have a negative excess area for all values of the line tension, and therefore, all lack sufficient area for repair. For the curved necks with a relatively low line tension value $\tilde{\tau} = 1$ shown in Fig. 3 *A*, one finds that the most narrow and constricted neck shapes are generated when the excess area is slightly positive (dark blue profile in Fig. 3 *A*). Since the model is formulated under a condition of constant membrane area, the area is the control parameter that can be independently set (rather than the membrane tension). This fact can be brought out in a representation of the neck shapes according to their excess area. Although the profiles in Fig. 3 were generated using varying tensions, they have different membrane areas, and one can shift representation by sorting the solutions according to their excess area as done in Fig. 4. Here, the *y* axis is the "relative energy" $\Delta\tilde{S}$ of the membrane relative to that of a flat membrane without a hole, but with spontaneous curvature. Each point in the state diagram of Fig. 4 represents a distinct neck shape for that particular area. It should also be noted that both curves in Fig. 4 contain a transition from negative to positive membrane tensions $\tilde{\sigma}$ in the direction indicated, whereas the total tension $\tilde{\sigma}_{\text{tot}}$ remains always positive. Having established the basis for constructing diagrams of neck shapes, we can proceed to construct a more complete state diagram by variation of the line tension. Fig. 5 shows the state diagram upon variation of the dimensionless line tension from $\tilde{\tau} = 1$–7 corresponding approximately to 2–14 pN in physical units. The curves in Fig. 5 *A* correspond to fixed values of the line tension, and within each curve, the membrane tension $\tilde{\sigma}$ varies in the direction indicated. The vertical displacement of the curves mainly originates from the variation in line tension energy $(2\pi r_1 \tau)$. Note that membrane states with the same line tension and area, but different energies, have been truncated to keep only the states with the lowest energy. This is, for instance, the case for the curved neck states approaching the limit $\Delta\tilde{A} = 0$ in Fig. 5 *A*, which can convert to flat neck conformations with a lower energy when the excess area becomes negative. The flat neck structures are located at negative excess area $\Delta\tilde{A} < 0$, and all approach a flat membrane without a hole for excess areas going to zero, i.e., the point (0,0) in Fig. 5 *A*. The change in shape of the flat necks with respect to varying excess area and tension is illustrated in Fig. 5 *C*, which also shows the approach to a flat sealed membrane. Note that to sustain infinitely small holes with $\Delta\tilde{A}<0$ requires a membrane tension $\tilde{\sigma}$ approaching infinity. Since this is not possible in practice, very small holes with negative excess area will spontaneously close, subject to the effect of line tension. If we consider the curved neck states

Please cite this article in press as: Klenow et al., Shape of the membrane neck around a hole during plasma membrane repair, Biophysical Journal (2024), https://doi.org/10.1016/j.bpj.2024.05.027

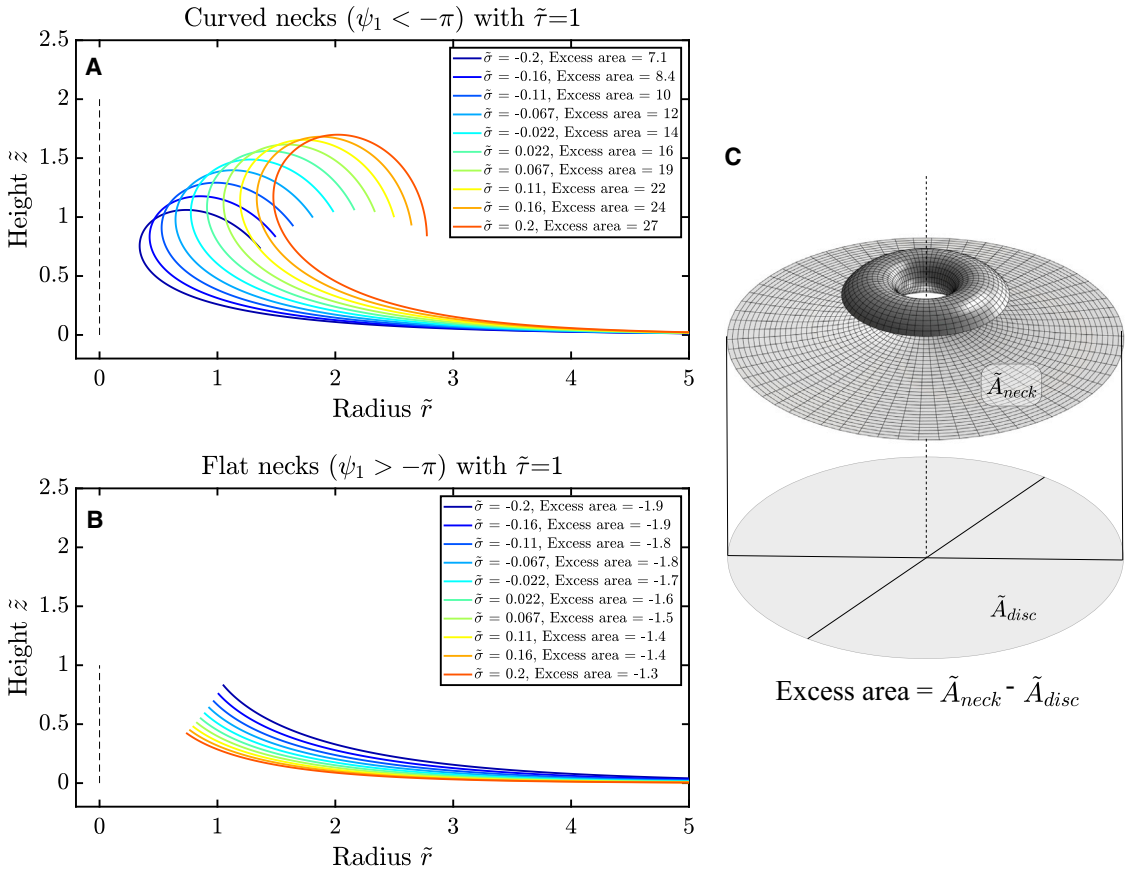

FIGURE 3 Examples of variations in neck shapes for line tension $\tilde{\tau} = 1$ where solutions with varying membrane area and corresponding membrane tension are shown. A curved (*A*) and a flat (*B*) group of neck shapes emerge when solving the shape equations, as was also shown in Fig. 2. The two types of solutions can be discriminated using, e.g., the cutoff $\psi_1 < -\pi$ and $\psi_1 > -\pi$, respectively. The excess area is defined as the membrane area minus the area of a corresponding flat disk (*C*). To see this figure in color, go online.

located at positive excess area ($\Delta\tilde{A}>0$) in Fig. 5 *A*, they all correspond to membrane conformations that in principle have sufficient membrane area for repair. Importantly, we find that the curved neck states only exist for line tension up to around $\tilde{\tau} = 5$ or approximately 10 pN. Examples of the variation in the shape of the curved neck are shown in Fig. 5 *B*. At high positive values of the excess area, the curved necks cease to exist because the membrane self-intersects (curve f in Fig. 5 *B*). At small positive values of the excess area, the curved neck states are terminated when the tension approaches the limit $\tilde{\sigma} \to -0.5$. The possibility of more narrow neck conformations as predicted by the model are of interest in a mechanism of plasma membrane repair, since narrow neck shapes could potentially be transition states to the sealed membrane. For this purpose, it is useful to reconstruct the state diagram with the neck radius plotted against the excess area as done in Fig. 6. Here, the neck radius is defined as the minimum radius of the membrane hole for a given neck shape. In Fig. 6 *A*, the flat necks with $\Delta\tilde{A}<0$ display a quite uniform behavior. By comparison with the reference curve for a hole in a planar membrane ($A = \pi r^2$), it is clear that flat neck structures for all line tensions approach the planar conformation when the hole is small, i.e., negative $\Delta\tilde{A} \simeq 0$, and the membrane has a high positive membrane tension. This behavior is illustrated with the membrane profiles (a,b) in Fig. 6 *B* corresponding to the points marked in Fig. 6 *A*. If we consider the curved necks at $\Delta\tilde{A}>0$ in Fig. 6 *A*, we note that the curves are terminated at a limit of high excess area due to self-intersection of the membrane. For intermediate positive excess areas ($\Delta\tilde{A} \simeq$ 0–40), Fig. 6 *A* shows a bifurcation behavior of the membrane states is observed consisting of an upper branch with larger neck radii and higher line tensions and a lower branch with more narrow necks and smaller line tensions. This behavior is illustrated by the points c ($\tilde{\tau} = 3.8$, $\tilde{\sigma} = 0.06$) and d ($\tilde{\tau} = 1.0$, $\tilde{\sigma} = -0.21$) where the corresponding profiles are plotted in Fig. 6 *B*. For comparison with Fig. 6 *A*, one could alternatively choose to plot the free edge radius $\tilde{r}_1$ against the excess area to bring out the role of the free edge. This was done in Figure S3 and shows qualitatively the same bifurcation behavior. The possible significance for membrane repair of the neck states with positive excess area is discussed below.

Please cite this article in press as: Klenow et al., Shape of the membrane neck around a hole during plasma membrane repair, Biophysical Journal (2024), https://doi.org/10.1016/j.bpj.2024.05.027

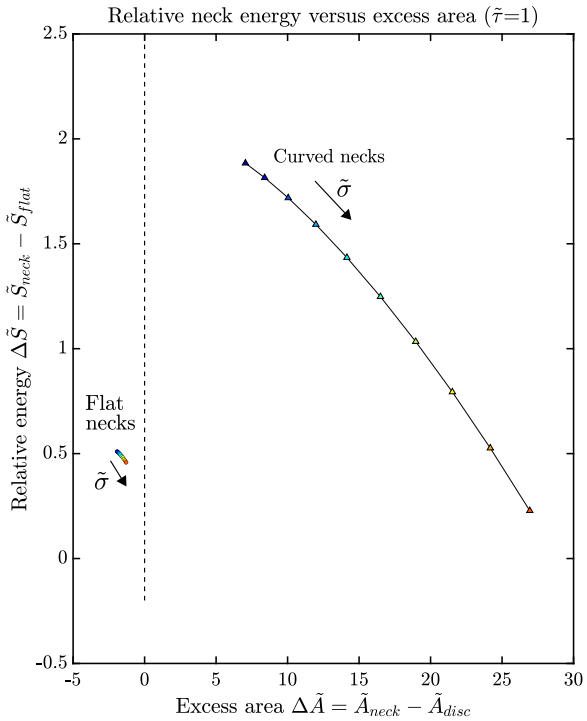

FIGURE 4 State diagram of the neck conformations in Fig. 3 in a representation of energy versus excess area. A neck conformation is represented by a point in the plot, with the same colors as in Fig. 3. The relative neck energy is computed as the total energy ($\tilde{S}$) minus the energy of flat, intact membrane with the same area and with spontaneous curvature. Arrows indicate the direction of increasing membrane tension $\tilde{\sigma}$. To see this figure in color, go online.

DISCUSSION

Considering the situation immediately after a rupture of the plasma membrane in a cell, the membrane has a negative excess area, and therefore, it lacks the necessary area for sealing the hole. Our model points to the existence of curved membrane conformations with a positive excess area that may have relevance in a mechanism of repair. The formation of such necks requires the supply of excess area to the damage site in the early phases of membrane repair. This agrees with the fact that area supply after damage is generally considered a prerequisite for successful membrane repair in cells (1,49–51). To this end, exocytosis of intracellular vesicles has been widely reported as a key source of membrane area during repair. Specifically, the exocytosis of lysosomes to the plasma membrane was shown to mediate repair (52,53), and recently, the fusion of early endosomes was also shown to contribute membrane area during repair (54). Area supply has been associated with a reduction of the membrane tension, and Togo et al. showed that a decrease in plasma membrane tension precedes successful repair of membrane injuries (55). Also, membrane tension and the availability of excess membrane area correlates strongly with the attachment/detachment of cortical actin to the plasma membrane as measured with AFM in cells (56,57). Our model implies that negative values of the membrane tension ($\tilde{\sigma} < 0$) are associated with some of the neck conformations. However, due to the contribution from spontaneous tension arising from the spontaneous membrane curvature, the total membrane tension ($\tilde{\sigma}_{\mathrm{tot}} = \tilde{\sigma} + 1/2$) remains positive for all conformations. A reduction of the line tension at the free edge to or below 1 pN is associated with the more constricted necks in our model. It was previously shown that Tween 20 can lower line tension in DOPC membranes down to 0.2 pN (43), and increased leakage from pores in the presence of lysolipids has also been demonstrated (58). Taking into account the compositional complexity of the cytosol, we hypothesize that biological surfactants could reduce line tension in cells by an equivalent surfactant-binding mechanism. But further experiments are required to quantify the line tension of plasma membrane edges under realistic conditions in cells. The numeric solutions to the shape equations fulfill the requirement $dS = 0$ of zero variation in the total energy. This is a necessary condition for a stable energy minimum, but it is also fulfilled at saddle points or maxima. Previous studies using a similar variational approach have assumed stability without performing a rigorous stability analysis (19,59). Even though we have selected minimum energy configurations among the solutions to the shape equations for a given excess area, we have not done a full stability analysis. Thus, we cannot be certain that the solutions we have found are all stable or metastable. In particular, one could speculate that solutions found at positive excess area are saddle points. This is based on the argument that for some of these configurations (Figure S3) an increase in the free edge radius $\tilde{r}_1$ is balanced by an increase in line tension. Thus, when this increase in line tension does not happen, then the edge radius could spontaneously increase further. Note that the converse of this statement is that an edge radius $\tilde{r}_1$ below the value for the solution of the shape equations will shrink toward zero. If this is the case, then the solutions found instead indicate maximal holes that the biomembrane should avoid surpassing, in order to not tear open, and that holes below this size are unstable against constriction/closing. Based on the model, a possible scenario emerges for membrane remodeling during plasma membrane repair. To illustrate these concepts, Fig. 7 *A* shows the plasma membrane as viewed from the intracellular side immediately after a rupture. At this time point, the membrane has a negative excess area, preventing sealing of the hole. Injury is immediately followed by influx of calcium ions into the cytosol, activating the repair machinery including membrane binding of annexins and the generation of spontaneous membrane curvature near the site of damage. Depolymerization of cortical actin and the fusion of early endosomes with the plasma contribute to the supply of membrane area and result in a positive excess area near the damage site, as indicated in Fig. 7 *B*. Additionally, a change in line tension may occur via adsorption of surfactants to the free edge. The

Please cite this article in press as: Klenow et al., Shape of the membrane neck around a hole during plasma membrane repair, Biophysical Journal (2024), https://doi.org/10.1016/j.bpj.2024.05.027

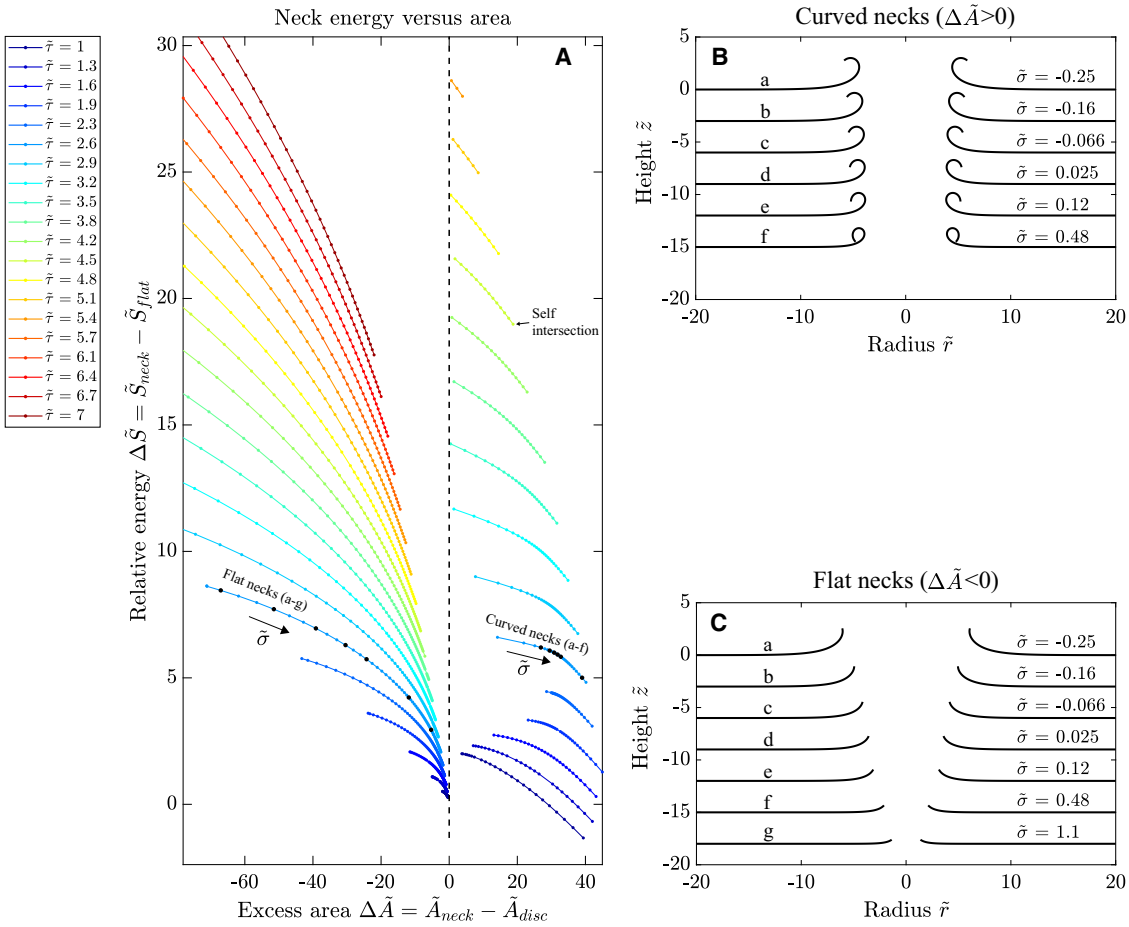

FIGURE 5 Extended state diagram of neck shapes in representation of energy versus area, for a range of line tensions ($\tilde{\tau} = 1$–7) color coded as indicated in the legend (*A*). Examples of curved and flat neck shapes (with $\tilde{\tau} = 2.6$) are shown in (*B*) and (*C*) respectively, with the corresponding values of the membrane tension $\tilde{\sigma}$ indicated. The lines representing curved neck shapes were truncated at high $\Delta\tilde{A}$ values when the membrane self-intersects. Multiple states with the same area and line tension, but different energy, were truncated to keep only the state with the lowest energy. To see this figure in color, go online.

combination of spontaneous curvature, supply of excess area, and change in line tension will lead to membrane remodeling around the hole. The model predicts curved and constricted membrane conformations having zero variation in the energy. However, transiently unstable conformations could also be created that are not described by the shape equations but that are relevant for repair. As indicated above, unstable states with a smaller hole size than the shape solutions could be unstable against neck constriction. The sealing of the membrane hole requires a change in membrane topology that is not predicted by the model. However, a possible route to sealing is either the spontaneous or the protein-assisted fission of a narrow neck in a process analogous to vesicle fission/division. Neck fission and sealing of the hole would lead to the internalization of membrane fragments containing the membrane region that was closest to the hole edge. The fragments are possibly entering internal recycling, and the process may be related to the phenomenon of "LC3-associated macropinocytosis" after membrane repair, as was previously reported (60). Membrane fission is widely present in nature and is essential for maintaining cellular life. Fission occurs via the progressive constriction of a membrane neck by either passive or active processes (61). As reviewed by Renard et al. (62), passive constriction may typically occur via spontaneous curvature mechanisms, whereas active constriction can, e.g., be induced by members of the dynamin family or by ESCRT complexes. Constriction below a threshold neck radius induces a so-called hemifission intermediate state where internal monolayers of the membrane neck are fused. The hemifission state is believed to decay spontaneously into two separate membranes, completing the fission process. A curvature elastic model for fission by Kozlovsky and Kozlov (63) predicts that under a critical neck diameter of 4–5 nm, the hemifission state (i.e., fission) becomes energetically favored over the neck structure. Experimentally, the diameter of the fission pore has been estimated to be near 4 nm (64). The diameter of a membrane tube constricted by an outer helical assembly of dynamin was determined to 3.7 nm by cryo-EM (65). Although our model predicts the existence of narrow necks under certain configurations, further studies are needed to decide if such conformations can

Please cite this article in press as: Klenow et al., Shape of the membrane neck around a hole during plasma membrane repair, Biophysical Journal (2024), https://doi.org/10.1016/j.bpj.2024.05.027

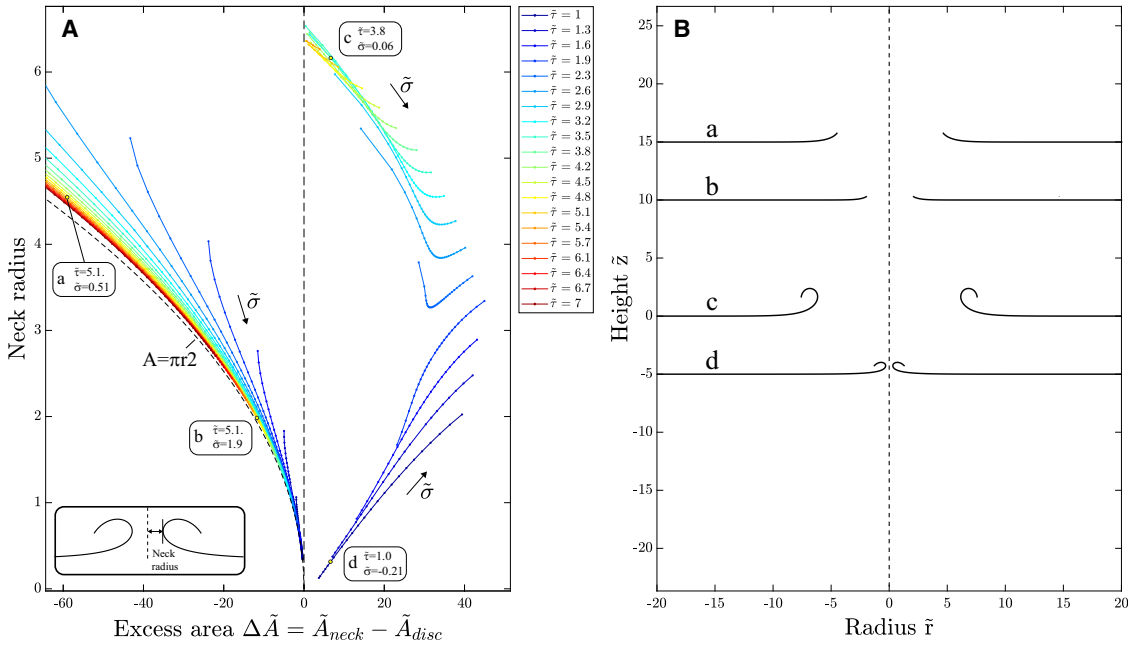

FIGURE 6 State diagram of neck profiles in Fig. 5 in a representation of neck radius versus excess area (A). Neck radius is defined as the minimum radius of the membrane hole as indicated in the insert. For the flat necks at $\Delta\tilde{A}<0$, the excess area and radius of a planar membrane with circular hole is plotted for comparison ($A = \pi r^2$). The flat necks approach the planar conformation for negative excess areas close to zero and high membrane tensions as indicated in (B) point *a,b*. The curved neck states with $\Delta\tilde{A}>0$ are split into a branch with higher neck radii and a branch with lower neck radii (A). The difference between these two branches is illustrated by the points *c* and *d* and the corresponding neck shapes in (B). To see this figure in color, go online.

spontaneously undergo fission, or if active constriction is required to complete fission. Interestingly, the osmotic manipulation of GUVs resulting in smaller vesicles has demonstrated membrane fission in highly simplistic systems, further illustrating the wide range of conditions under which fission can occur (66). The membrane recruitment of curvature-inducing annexins after damage is required for formation of a neck around the hole. Several members of the annexin family are implicated in repair with ANXA4 and ANXA5 arriving early and being strong inducers of curvature as evidenced by the induction of membrane rolling of planar membranes (12,67). Moreover, both ANXA4 (68) and ANXA5 (10) have been shown to bind to negatively curved membranes, creating the possibility for a self-amplifying effect that could further enhance the formation of local curvature in the neck. Although the model presented here assumes the spontaneous curvature to be uniformly distributed over the membrane surface, an extended description could also incorporate a nonuniform lateral annexin distribution and the possible interplay between the membrane shape and the local annexin density. An additional effect of annexins is the cross-linking of adjacent membrane surfaces promoted by ANAA1, ANXA2, and ANXA6, where the latter has been shown to act in concert with ANXA4 to assist wound closure during repair (11). We have demonstrated the joint effect of curvature induction by ANXA4

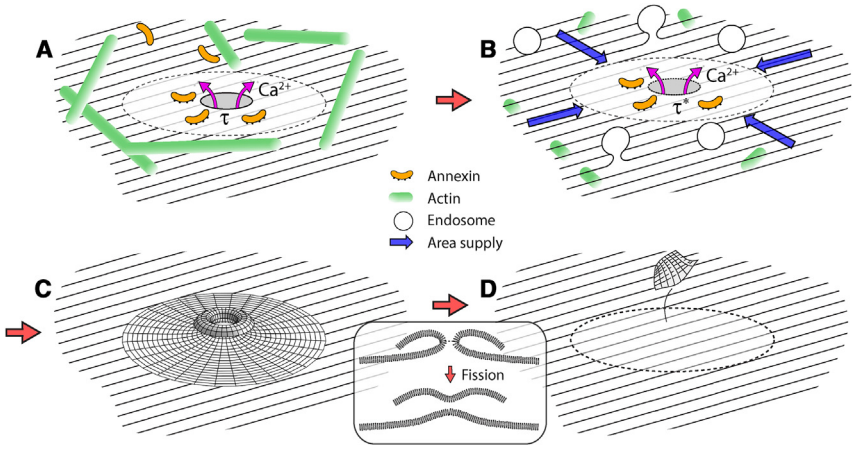

FIGURE 7 Illustration of a possible scenario for membrane repair as driven by membrane curvature and supply of excess membrane area. A membrane hole promotes the influx of Ca^{2+} and membrane binding of curvature-inducing annexins (A). Supply of excess membrane area to the hole may occur by mechanisms such as actin depolymerization and fusion of early endosomes (B). According to the present model, the combined effect of curvature, supply of excess membrane area, and a reduction of line tension ($\tau \rightarrow \tau^*$) can promote a curved and constricted neck geometry (C). The neck may potentially undergo spontaneous or protein-assisted membrane fission, leading to sealing of the hole and the shedding of a membrane fragment for internal recycling (D). To see this figure in color, go online.

Please cite this article in press as: Klenow et al., Shape of the membrane neck around a hole during plasma membrane repair, Biophysical Journal (2024), https://doi.org/10.1016/j.bpj.2024.05.027

and the cross-linking by ANXA6 in a combined study using planar membranes (69). These results further support the notion that ANXA6, containing two membrane-binding core domains, could also modulate the neck shape to promote fission and hole sealing.

CONCLUSION

In conclusion, we have formulated and solved an idealized mechanical model for the membrane shape near a hole during plasma membrane repair. The model predicts that the combination of spontaneous curvature and line tension under a fixed area constraint leads to membrane remodeling and the creation of neck structures around a hole as mapped out in a state diagram. Without the supply of additional membrane area after damage, only a weakly curved morphology around the hole is possible. Supply of excess membrane area near the hole enables the formation of more curved neck conformations. The model indicates that narrow and curved neck structures may be potential transition states to a membrane fission event that eventually seals the membrane hole. Since plasma membrane repair must occur on a timescale of seconds (16) to maintain cellular homeostasis, the mechanical remodeling of membrane shapes by spontaneous curvature and line tension provides a potential mechanism for repair.

SUPPORTING MATERIAL

Supporting Material can be found online at https://doi.org/10.1016/j.bpj.2024.05.027.

AUTHOR CONTRIBUTIONS

M.B.K., A.C.S., M.A.L., W.P., and J.N. formulated the model based on input from cell studies by J.N. A.C.S., M.B.K., M.A.L., M.S.V., and W.P. performed the analytical calculations. A.C.S. and M.S.V. performed the numeric implementation, and A.C.S. wrote the manuscript.

ACKNOWLEDGMENTS

We thank the Independent Research Fund Denmark (DFF) for support via grant no. 7014-00036B and the Novo Nordisk Foundation via grant no. NNF18OC0034936.

DECLARATION OF INTERESTS

The authors declare no competing interests.

REFERENCES

1. Moe, A. M., A. E. Golding, and W. M. Bement. 2015. Cell healing: Calcium, repair and regeneration. *Semin. Cell Dev. Biol.* 45:18–23.
2. Heilbrunn, L. 1930. The surface precipitation reaction of living cells. *In* Proceedings of the American Philosophical Society, *69*, pp. 295–301.
3. Horn, A., and J. K. Jaiswal. 2018. Cellular mechanisms and signals that coordinate plasma membrane repair. *Cell. Mol. Life Sci.* 75:3751–3770.
4. Cooper, S. T., and P. L. McNeil. 2015. Membrane repair: mechanisms and pathophysiology. *Physiol. Rev.* 95:1205–1240.
5. Li, Z., and G. S. Shaw. 2023. Role of calcium-sensor proteins in cell membrane repair. *Biosci. Rep.* 43: BSR20220765.
6. Draeger, A., K. Monastyrskaya, and E. B. Babiychuk. 2011. Plasma membrane repair and cellular damage control: the annexin survival kit. *Biochem. Pharmacol.* 81:703–712.
7. Boye, T. L., and J. Nylandsted. 2016. Annexins in plasma membrane repair. *Biol. Chem.* 397:961–969.
8. Bendix, P. M., A. C. Simonsen, …, J. Nylandsted. 2020. Interdisciplinary Synergy to Reveal Mechanisms of Annexin-Mediated Plasma Membrane Shaping and Repair. *Cells.* 9:1029.
9. Hakobyan, D., V. Gerke, and A. Heuer. 2017. Modeling of annexin A2 - Membrane interactions by molecular dynamics simulations. *PLoS One.* 12: e0185440.
10. Moreno-Pescador, G., C. D. Florentsen, …, P. M. Bendix. 2019. Curvature- and Phase-Induced Protein Sorting Quantified in Transfected Cell-Derived Giant Vesicles. *ACS Nano.* 13:6689–6701.
11. Boye, T. L., K. Maeda, …, J. Nylandsted. 2017. Annexin A4 and A6 induce membrane curvature and constriction during cell membrane repair. *Nat. Commun.* 8: 1623.
12. Boye, T. L., J. C. Jeppesen, …, A. C. Simonsen. 2018. Annexins induce curvature on free-edge membranes displaying distinct morphologies. *Sci. Rep.* 8, 10309.
13. Portet, T., and R. Dimova. 2010. A new method for measuring edge tensions and stability of lipid bilayers: effect of membrane composition. *Biophys. J.* 99:3264–3273.
14. Shi, Z., Z. T. Graber, …, A. E. Cohen. 2018. Cell membranes resist flow. *Cell.* 175:1769–1779.e13.
15. Cohen, A. E., and Z. Shi. 2020. Do cell membranes flow like honey or jiggle like jello? *Bioessays.* 42: 1900142.
16. Klenow, M. B., A. S. B. Heitmann, A. C. Simonsen…, 2021. Timescale of hole closure during plasma membrane repair estimated by calcium imaging and numerical modeling. *Sci. Rep.* 11:4226.
17. Ebstrup, M. L., C. Dias, …, J. Nylandsted. 2021. Actin cytoskeletal dynamics in single-cell wound repair. *Int. J. Mol. Sci.* 22: 10886.
18. Helfrich, W. 1973. Elastic properties of lipid bilayers: theory and possible experiments. *Z. Naturforsch.* 28:693–703.
19. Seifert, U., K. Berndl, and R. Lipowsky. 1991. Shape transformations of vesicles: Phase diagram for spontaneous-curvature and bilayer-coupling models. *Phys. Rev.* 44:1182–1202.
20. Jülicher, F., and U. Seifert. 1994. Shape equations for axisymmetric vesicles: a clarification. *Phys. Rev.* 49:4728–4731.
21. Seifert, U. 1997. Configurations of fluid membranes and vesicles. *Adv. Phys.* 46:13–137.
22. Harden, J. L., F. C. MacKintosh, and P. D. Olmsted. 2005. Budding and domain shape transformations in mixed lipid films and bilayer membranes. *Phys. Rev.* 72: 011903.
23. Foret, L. 2014. Shape and energy of a membrane bud induced by protein coats or viral protein assembly. *Eur. Phys. J. E Soft Matter.* 37:42.
24. Kumar, G., and A. Sain. 2016. Shape transitions during clathrin-induced endocytosis. *Phys. Rev. E.* 94: 062404.
25. Yi, X., X. Shi, and H. Gao. 2011. Cellular uptake of elastic nanoparticles. *Phys. Rev. Lett.* 107: 098101.
26. Kusumaatmaja, H., and R. Lipowsky. 2011. Droplet-induced budding transitions of membranes. *Soft Matter.* 7:6914–6919.
27. Deslandes, F., A. R. Thiam, and L. Forêt. 2017. Lipid Droplets Can Spontaneously Bud Off from a Symmetric Bilayer. *Biophys. J.* 113:15–18.

Please cite this article in press as: Klenow et al., Shape of the membrane neck around a hole during plasma membrane repair, Biophysical Journal (2024), https://doi.org/10.1016/j.bpj.2024.05.027

28. Chabanon, M., and P. Rangamani. 2018. Gaussian curvature directs the distribution of spontaneous curvature on bilayer membrane necks. *Soft Matter.* 14:2281–2294.
29. Agrawal, A., and D. J. Steigmann. 2009. Modeling protein-mediated morphology in biomembranes. *Biomech. Model. Mechanobiol.* 8:371–379.
30. Tu, Z. C., and Z. C. Ou-Yang. 2003. Lipid membranes with free edges. *Phys. Rev.* 68: 061915.
31. Ni, D., H. Shi, and Y. Yin. 2005. Theoretical analysis of adhering lipid vesicles with free edges. *Colloids Surf. B Biointerfaces.* 46:162–168.
32. Umeda, T., Y. Suezaki, …, H. Hotani. 2005. Theoretical analysis of opening-up vesicles with single and two holes. *Phys. Rev.* 71: 011913.
33. Tu, Z. C. 2010. Compatibility between shape equation and boundary conditions of lipid membranes with free edges. *J. Chem. Phys.* 132: 084111.
34. Yao, Z., R. Sknepnek, …, M. Olvera de la Cruz. 2012. Shapes of pored membranes. *Soft Matter.* 8:11613–11619.
35. Zhou, X. 2019. Boundary behaviour of open vesicles in axisymmetric case. *J. Phys. Condens. Matter.* 31: 315101.
36. Rangamani, P. 2022. The many faces of membrane tension: Challenges across systems and scales. *Biochim. Biophys. Acta Biomembr.* 1864: 183897.
37. Lipowsky, R. 2013. Spontaneous tubulation of membranes and vesicles reveals membrane tension generated by spontaneous curvature. *Faraday Discuss.* 161:305–459.
38. Dasgupta, R., M. S. Miettinen, …, R. Dimova. 2018. The glycolipid GM1 reshapes asymmetric biomembranes and giant vesicles by curvature generation. *Proc. Natl. Acad. Sci. USA.* 115:5756–5761.
39. Roy, D., J. Steinkühler, …, R. Dimova. 2020. Mechanical Tension of Biomembranes Can Be Measured by Super Resolution (STED) Microscopy of Force-Induced Nanotubes. *Nano Lett.* 20:3185–3191.
40. Steinkühler, J., E. Sezgin, …, R. Dimova. 2019. Mechanical properties of plasma membrane vesicles correlate with lipid order, viscosity and cell density. *Commun. Biol.* 2:337.
41. Chen, Z., Y. Mao, …, H. Yang. 2014. Characterizing the binding of annexin V to a lipid bilayer using molecular dynamics simulations. *Proteins.* 82:312–322.
42. Pandey, M. P., P. C. Telles de Souza, …, H. Khandelia. 2024. Bending of a lipid membrane edge by annexin A5 trimers. *Biophys. J.* 123:1006–1014.
43. Karatekin, E., O. Sandre, …, F. Brochard-Wyart. 2003. Cascades of transient pores in giant vesicles: line tension and transport. *Biophys. J.* 84:1734–1749.
44. Tazawa, K., and M. Yamazaki. 2023. Effect of monolayer spontaneous curvature on constant tension-induced pore formation in lipid bilayers. *J. Chem. Phys.* 158: 081101.
45. Evans, E., W. Rawicz, and B. A. Smith. 2013. Back to the future: mechanics and thermodynamics of lipid biomembranes. *Faraday Discuss.* 161:591–611.
46. Peukes, J., and T. Betz. 2014. Direct measurement of the cortical tension during the growth of membrane blebs. *Biophys. J.* 107:1810–1820.
47. Tinevez, J.-Y., U. Schulze, …, E. Paluch. 2009. Role of cortical tension in bleb growth. *Proc. Natl. Acad. Sci. USA.* 106:18581–18586.
48. Pradhan, S., M. A. K. Williams, and T. K. Hale. 2022. Changes in the properties of membrane tethers in response to hp1α depletion in mcf7 cells. *Biochem. Biophys. Res. Commun.* 587:126–130.
49. Davenport, N. R., and W. M. Bement. 2016. Cell repair: Revisiting the patch hypothesis. *Commun. Integr. Biol.* 9, e1253643.
50. Andrews, N. W., and M. Corrotte. 2018. Plasma membrane repair. *Curr. Biol.* 28:R392–R397.
51. Dias, C., and J. Nylandsted. 2021. Plasma membrane integrity in health and disease: significance and therapeutic potential. *Cell Discov.* 7:4–18.
52. Reddy, A., E. V. Caler, and N. W. Andrews. 2001. Plasma membrane repair is mediated by Ca2+-regulated exocytosis of lysosomes. *Cell.* 106:157–169.
53. Jaiswal, J. K., N. W. Andrews, and S. M. Simon. 2002. Membrane proximal lysosomes are the major vesicles responsible for calcium-dependent exocytosis in nonsecretory cells. *J. Cell Biol.* 159:625–635.
54. Raj, N., L. Greune, …, V. Gerke. 2023. Early Endosomes Act as Local Exocytosis Hubs to Repair Endothelial Membrane Damage. *Adv. Sci.* 10: e2300244.
55. Togo, T., T. B. Krasieva, and R. A. Steinhardt. 2000. A decrease in membrane tension precedes successful cell-membrane repair. *Mol. Biol. Cell.* 11:4339–4346.
56. Rouven Brückner, B., A. Pietuch, …, A. Janshoff. 2015. Ezrin is a major regulator of membrane tension in epithelial cells. *Sci. Rep.* 5: 14700.
57. Chugh, P., A. G. Clark, …, E. K. Paluch. 2017. Actin cortex architecture regulates cell surface tension. *Nat. Cell Biol.* 19:689–697.
58. Ralston, E., R. Blumenthal, …, P. Henkart. 1980. Lysophosphatidylcholine in liposomal membranes. Enhanced permeability but little effect on transfer of a water-soluble fluorescent marker into human lymphocytes. *Biochim. Biophys. Acta.* 597:543–551.
59. Bozic, B., S. Svetina, and B. Zeks. 1997. Theoretical analysis of the formation of membrane microtubes on axially strained vesicles. *Phys. Rev. E.* 55:5834–5842.
60. Sønder, S. L., S. C. Häger, …, J. Nylandsted. 2021. Restructuring of the plasma membrane upon damage by LC3-associated macropinocytosis. *Sci. Adv.* 7: eabg1969.
61. Frolov, V. A., A. Escalada, …, A. V. Shnyrova. 2015. Geometry of membrane fission. *Chem. Phys. Lipids.* 185:129–140.
62. Renard, H.-F., L. Johannes, and P. Morsomme. 2018. Increasing diversity of biological membrane fission mechanisms. *Trends Cell Biol.* 28:274–286.
63. Kozlovsky, Y., and M. M. Kozlov. 2003. Membrane fission: model for intermediate structures. *Biophys. J.* 85:85–96.
64. María Cabeza, J., J. Acosta, and E. Alés. 2010. Dynamics and regulation of endocytotic fission pores: role of calcium and dynamin. *Traffic.* 11:1579–1590.
65. Sundborger, A. C., S. Fang, …, J. E. Hinshaw. 2014. A dynamin mutant defines a superconstricted prefission state. *Cell Rep.* 8:734–742.
66. Liu, X., J. Stenhammar, …, E. Sparr. 2022. Vesicles balance osmotic stress with bending energy that can be released to form daughter vesicles. *J. Phys. Chem. Lett.* 13:498–507.
67. Mularski, A., S. L. Sønder, …, A. C. Simonsen. 2021. Simultaneous membrane binding of Annexin A4 and A5 suppresses 2D lattice formation while maintaining curvature induction. *J. Colloid Interface Sci.* 600:854–864.
68. Florentsen, C. D., A. Kamp-Sonne, …, P. M. Bendix. 2021. Annexin A4 trimers are recruited by high membrane curvatures in giant plasma membrane vesicles. *Soft Matter.* 17:308–318.
69. Mularski, A., S. L. Sønder, …, A. C. Simonsen. 2022. Interplay of membrane crosslinking and curvature induction by annexins. *Sci. Rep.* 12: 22568.

Biophysical Journal, Volume *123*

Supplemental information

Shape of the membrane neck around a hole during plasma membrane repair

Martin Berg Klenow, Magnus Staal Vigsø, Weria Pezeshkian, Jesper Nylandsted, Michael Andersen Lomholt, and Adam Cohen Simonsen

Supplementary material for:
Shape of the membrane neck around a hole during plasma membrane repair

1 Definitions and assumptions

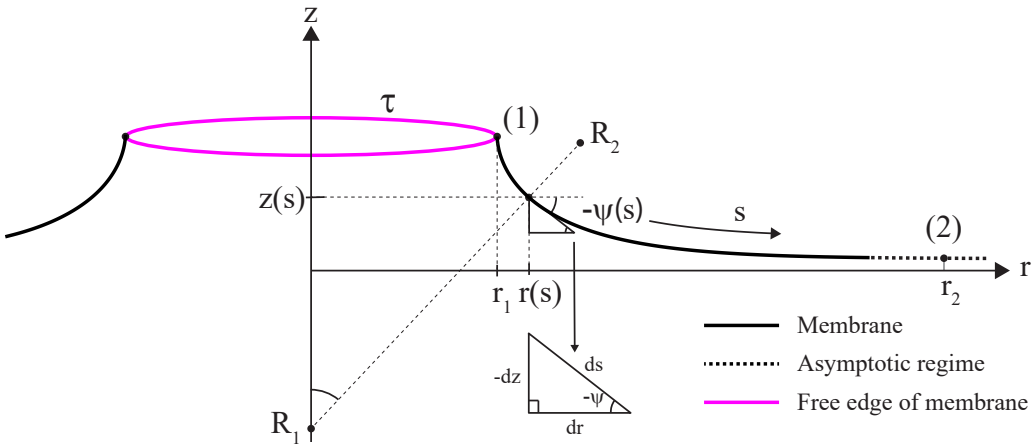

Figure S1: Geometry and definitions in a model for membrane curvature around a circular hole. The neck shape is given by coordinates $r(s)$, $z(s)$ and $\psi(s)$ which are functions of the arc length s.

We aim to model the membrane shape near a hole using the simplifying assumption of axial symmetry. Upon plasma membrane rupture and Ca^{2+}influx, binding of curvature-inducing proteins generates a spontaneous curvature (c_0) of the membrane. The combined effects of spontaneous curvature, membrane tension and line tension (τ) at the free edge results in a curved conformation of the membrane near the region of the hole described by coordinates $r(s)$, $z(s)$ and the angle $\psi(s)$ with s being the arc length. The equilibrium conformations of the membrane near the hole is determined through variational calculus of the total energy functional.

2 Energy of the neck conformation

The free energy of the membrane neck is the sum of the Helfrich energy plus a contribution from line tension at the free membrane edge:

$$G_{\text{neck}} = \int_A \left[\frac{k}{2}(2H - c_0)^2 + k_G K\right] dA + 2\pi\tau r_1 \tag{S.1}$$

Here $2H$ is the total curvature and H is the mean curvature, c_0 is the spontaneous total curvature, K is the Gaussian curvature, k is the bending modulus, k_G is the Gaussian curvature modulus and $r_1 = r(s_1)$ is the radius at the hole edge. The area integration is over a sufficiently large area A away from the hole that state (2) can be considered to lie in the asymptotic regime. It is useful to parameterize the shape coordinates by the arc length s, defined to be increasing when traveling away from the membrane free edge. The system is subject to the following geometrical constraints on the coordinates: $r(s)$, $z(s)$ and

$\psi(s)$:

$$\frac{dz}{ds} = \dot{z} = \sin\psi \tag{S.2}$$

$$\frac{dr}{ds} = \dot{r} = \cos\psi \tag{S.3}$$

The total curvature $2H$ and the Gaussian curvature K are expressed in terms of the principal curvature radii R_1, R_2 as:

$$2H = \frac{1}{R_1} + \frac{1}{R_2} = \dot{\psi} + \frac{\sin\psi}{r} \tag{S.4}$$

$$K = \frac{1}{R_1 R_2} = \dot{\psi}\frac{\sin\psi}{r} \tag{S.5}$$

Using the area element $dA = 2\pi r ds$ and defining the energy functional S, equation (S.1) becomes:

$$\frac{G_{\text{neck}}}{2\pi} = S = \int_{s_1}^{s_2} \left[\frac{k}{2}\left(\dot{\psi} + \frac{\sin\psi}{r} - c_0\right)^2 r + k_G\dot{\psi}\sin\psi\right] ds + \tau r_1 \tag{S.6}$$

The Gaussian curvature term is integrated to yield:

$$S = \int_{s_1}^{s_2} \mathcal{L}_0 ds - k_G\cos\psi|_{s_1}^{s_2} + \tau r_1 \tag{S.7}$$

where the 'Lagrangian' function ($\mathcal{L}_0$) has been defined as:

$$\mathcal{L}_0 = \frac{k}{2}\left(\dot{\psi} + \frac{\sin\psi}{r} - c_0\right)^2 r \tag{S.8}$$

To achieve mechanical equilibrium, the membrane is allowed to have a constant, non-zero tension (σ). The tension energy G_{tension} associated with an area change $A - A_0$, can be written:

$$G_{\text{tension}} = \sigma(A - A_0) = 2\pi\int_{s_1}^{s_2} \sigma r ds - \sigma A_0 \tag{S.9}$$

The tension (σ) can be regarded as a Lagrange multiplier for the requirement of constant area. When applying variational calculus to the energy functional (below), the constant area term A_0 does not enter. According to equation (S.9) it means that the membrane tension only contributes with a term σr to the Lagrangian. The membrane is also subject to the geometrical constraints (S.2,S.3) which further generates two Lagrange multipliers: $t(s)$ and $v(s)$. In total, the full Lagrangian relevant for energy minimization becomes:

$$\mathcal{L} = \frac{k}{2}\left(\dot{\psi} + \frac{\sin\psi}{r} - c_0\right)^2 r + t(\dot{r} - \cos\psi) + v(\dot{z} - \sin\psi) + \sigma r \tag{S.10}$$

3 Energy minimization

The total energy functional is written as:

$$S = \int_{s_1}^{s_2} \mathcal{L}\, ds - k_G\cos\psi|_{s_1}^{s_2} + \tau r_1 \tag{S.11}$$

The equilibrium conformation of the membrane is established using variational calculus with the requirement that $\delta S = 0$. The total variation δS is:

$$\begin{aligned}\delta S = &\int_{s_1}^{s_2}\left[\left(\frac{\partial\mathcal{L}}{\partial\psi} - \frac{d}{ds}(\frac{\partial\mathcal{L}}{\partial\dot{\psi}})\right)\delta\psi + \left(\frac{\partial\mathcal{L}}{\partial r} - \frac{d}{ds}(\frac{\partial\mathcal{L}}{\partial\dot{r}})\right)\delta r + \left(\frac{\partial\mathcal{L}}{\partial z} - \frac{d}{ds}(\frac{\partial\mathcal{L}}{\partial\dot{z}})\right)\delta z\right] ds \\ &- \mathcal{H}\,\delta s|_{s_1}^{s_2} + \frac{\partial\mathcal{L}}{\partial\dot{\psi}}\delta\psi|_{s_1}^{s_2} + \frac{\partial\mathcal{L}}{\partial\dot{r}}\delta r|_{s_1}^{s_2} + \frac{\partial\mathcal{L}}{\partial\dot{z}}\delta z|_{s_1}^{s_2} + k_G\sin\psi\delta\psi|_{s_1}^{s_2} + \tau\delta r_1 \\ &= 0\end{aligned} \tag{S.12}$$

The three Euler-Lagrange terms in equation (S.12) must vanish separately at equilibrium, leading to the following differential equations:

$$\frac{\partial \mathcal{L}}{\partial \psi} - \frac{d}{ds}\left(\frac{\partial \mathcal{L}}{\partial \dot{\psi}}\right) = 0 \tag{S.13}$$

$$\Downarrow$$

$$\ddot{\psi} = -\dot{\psi}\frac{\cos\psi}{r} + \frac{\sin\psi\cos\psi}{r^2} + t\frac{\sin\psi}{kr} - v\frac{\cos\psi}{kr} \tag{S.14}$$

$$\frac{\partial \mathcal{L}}{\partial r} - \frac{d}{ds}\left(\frac{\partial \mathcal{L}}{\partial \dot{r}}\right) = 0 \tag{S.15}$$

$$\Downarrow$$

$$\dot{t} = \frac{k}{2}\left[(\dot{\psi} - c_0)^2 - \frac{\sin^2\psi}{r^2}\right] + \sigma \tag{S.16}$$

$$\frac{\partial \mathcal{L}}{\partial z} - \frac{d}{ds}\left(\frac{\partial \mathcal{L}}{\partial \dot{z}}\right) = 0 \tag{S.17}$$

$$\Downarrow$$

$$\dot{v} = 0 \tag{S.18}$$

The Hamiltonian $\mathcal{H}$ in equation(S.12) is:

$$\begin{aligned}\mathcal{H} &= -\mathcal{L} + \dot{\psi}\frac{\partial \mathcal{L}}{\partial \dot{\psi}} + \dot{r}\frac{\partial \mathcal{L}}{\partial \dot{r}} + \dot{z}\frac{\partial \mathcal{L}}{\partial \dot{z}} \\ &= \frac{kr}{2}\dot{\psi}^2 - \frac{kr}{2}\left(\frac{\sin\psi}{r} - c_0\right)^2 + t\cos\psi - v\sin\psi - \sigma r = 0\end{aligned} \tag{S.19}$$

Equation (S.19) arises due to endpoint variations of s in the variational calculus of S. The relation $\mathcal{H}$=0 is e.g. useful for obtaining relations between the coordinates.

The boundary terms in equation (S.12) must be zero for all variations at the boundaries. Since we will use the exact asymptotic solution for the membrane shape far away from the hole at $s = s_2$ (see below), the variations at this boundary are zero: $\delta\psi_2 = 0$, $\delta r_2 = 0$, $\delta z_2 = 0$.

At the membrane hole $s = s_1$, the boundary terms in equation (S.12) reduce to the following equation:

$$-\left(\frac{\partial \mathcal{L}}{\partial \dot{\psi}}|_{s_1} + k_G\sin\psi_1\right)\delta\psi_1 + \left(\tau - \frac{\partial \mathcal{L}}{\partial \dot{r}}|_{s_1}\right)\delta r_1 - \frac{\partial \mathcal{L}}{\partial \dot{z}}|_{s_1}\delta z_1 = 0 \tag{S.20}$$

The three terms in equation (S.20) must vanish separately, giving the following equations:

$$\dot{\psi}_1 = c_0 - \left(1 + \frac{k_G}{k}\right)\frac{\sin\psi_1}{r_1} \;\Leftrightarrow\; k_G = k\left[(c_0 - \dot{\psi}_1)\frac{r_1}{\sin\psi_1} - 1\right] \tag{S.21}$$

$$t(s_1) = t_1 = \tau \tag{S.22}$$

$$v(s_1) = 0 \tag{S.23}$$

Equation (S.21) provides the connection between the membrane conformation at the free edge and the Gaussian curvature modulus k_G. Equation (S.22) provides a stop criterium for terminating integration. Equation (S.23) and (S.18) combined gives v(s)=0 for all s. In summary, the following set of coupled

shape equations must be solved to obtain the membrane conformation via the functions: r,ψ, $\dot{\psi}$, t, z:

$$\dot{r} = \cos\psi \tag{S.24}$$

$$\dot{\psi} = u \tag{S.25}$$

$$\dot{u} = -u\frac{\cos\psi}{r} + \frac{\sin\psi\cos\psi}{r^2} + t\frac{\sin\psi}{kr} \tag{S.26}$$

$$\dot{t} = \frac{k}{2}\left[(\dot{\psi} - c_0)^2 - \frac{\sin^2\psi}{r^2}\right] + \sigma \tag{S.27}$$

$$\dot{z} = \sin\psi \tag{S.28}$$

$$\dot{A} = 2\pi r \tag{S.29}$$

Here we have added equation (S.29) in order to determine the membrane area A. Additionally the following relationship between the variables exists:

$$\mathcal{H} = \frac{kr}{2}\dot{\psi}^2 - \frac{kr}{2}\left(\frac{\sin\psi}{r} - c_0\right)^2 + t\cos\psi - \sigma r = 0 \tag{S.30}$$

4 Asymptotic solution to shape equations

Numeric integration of the shape equations (S.24)-(S.29) requires a defined initial state. We take the initial state to be the point $s = s_2$ defined as being located far away from the hole. Luckily, an analytic solution to the shape equations in this asymptotic limit can be found. Below, we determine the asymptotic solution to the shape equations for large values of s. It is assumed that $\psi \to 0$ for $s \to \infty$. First, equation (S.26) is expanded to first order in ψ:

$$\ddot{\psi} \approx -\frac{\dot{\psi}}{r} + \frac{\psi}{r^2} + \frac{t\psi}{kr} \tag{S.31}$$

Next, t is found to zero'th order in ψ from either equation (S.27) or (S.30):

$$t \approx \left(\frac{k}{2}c_0^2 + \sigma\right) r \tag{S.32}$$

Upon insertion of equation (S.32) into (S.31), the following differential equation is found:

$$r^2\ddot{\psi} + r\dot{\psi} - \psi\left[1 + \frac{r^2}{\lambda^2}\right] = 0 \tag{S.33}$$

with $\frac{1}{\lambda^2} = \frac{c_0^2}{2} + \frac{\sigma}{k}$ and λ being a characteristic length scale in the asymptotic limit. Equation (S.33) is identified as the modified Bessel differential equation and the relevant solution is (using $ds = dr$):

$$\psi(\frac{r}{\lambda}) = C \cdot K_1(\frac{r}{\lambda}) \tag{S.34}$$

-where C is a constant and K_1 is a modified Bessel function of the second kind and order one. By differentiation of the solution in equation (S.34), $\dot{\psi}$ can be found as $\dot{\psi}(p) = \frac{C}{\lambda}(-K_0(p) - \frac{K_1(p)}{p})$ with $p = \frac{r}{\lambda}$.

5 Shape equations with dimensionless variables

The equations defining the membrane shape can be reformulated using dimensionless variables. This eliminates the parameters k, c_0 from the shape equations and makes it simpler to map the possible membrane configurations when fewer input variables are needed. The following characteristic quantities emerge:

Length scale: $l_c = \frac{1}{c_0}$
Tension: $\sigma_c = kc_0^2$
Line tension: $\tau_c = kc_0$
Energy: $E_c = k$

Dimensionless versions of the previously defined variables, as denoted with˜can now be used to reformulate the shape equations and the Hamiltonian:

$$\dot{\tilde{r}} = \cos\psi \tag{S.35}$$

$$\dot{\tilde{\psi}} = \tilde{u} \tag{S.36}$$

$$\dot{\tilde{u}} = -\tilde{u}\frac{\cos\psi}{\tilde{r}} + \frac{\sin\psi\cos\psi}{\tilde{r}^2} + \tilde{t}\frac{\sin\psi}{k\tilde{r}} \tag{S.37}$$

$$\dot{\tilde{t}} = \frac{1}{2}\left[(\dot{\psi}-1)^2 - \frac{\sin^2\psi}{\tilde{r}^2}\right] + \tilde{\sigma} \tag{S.38}$$

$$\dot{\tilde{z}} = \sin\psi \tag{S.39}$$

$$\dot{\tilde{A}} = 2\pi\tilde{r} \tag{S.40}$$

$$\tilde{\mathcal{H}} = \frac{\mathcal{H}}{kc_0} = \frac{\tilde{r}}{2}\dot{\psi}^2 - \frac{\tilde{r}}{2}\left(\frac{\sin\psi}{\tilde{r}} - 1\right)^2 + \tilde{t}\cos\psi - \tilde{\sigma}\tilde{r} = 0 \tag{S.41}$$

using the definitions: $\tilde{r} = rc_0$, $\tilde{z} = zc_0$, $\dot{\tilde{r}} = \frac{dr}{ds} = \dot{r}$, $\dot{\psi} = \dot{\tilde{\psi}}c_0$, $t = \tilde{t}kc_0$, $\dot{t} = \dot{\tilde{t}}kc_0^2$, $\sigma = \tilde{\sigma}kc_0^2$, $\tau = \tilde{\tau}kc_0$, $\tilde{A} = Ac_0^2$. The analytic solution (S.34) in the asymptotic limit becomes:

$$\psi(\frac{\tilde{r}}{\tilde{\lambda}}) = C \cdot K_1(\frac{\tilde{r}}{\tilde{\lambda}}) \tag{S.42}$$

with $\frac{1}{\tilde{\lambda}^2} = (\frac{1}{2} + \tilde{\sigma})$. Equation (S.21) and (S.22) for the Gaussian curvature becomes in dimensionless units:

$$\frac{k_G}{k} = \alpha = (1 - \dot{\psi}_1)\frac{\tilde{r}_1}{\sin\psi_1} - 1 \tag{S.43}$$

$$\tilde{t}(\tilde{s}_1) = \tilde{t}_1 = \tilde{\tau} \tag{S.44}$$

The Lagrangian of equation (S.10) becomes in dimensionless units:

$$\tilde{\mathcal{L}} = \frac{\mathcal{L}}{kc_0} = \frac{1}{2}\left(\dot{\tilde{\psi}} + \frac{\sin\psi}{\tilde{r}} - 1\right)^2 \tilde{r} + \tilde{t}(\dot{\tilde{r}} - \cos\psi) + \tilde{\sigma}\tilde{r} \tag{S.45}$$

and the energy functional corresponding to equation (S.11) becomes:

$$\tilde{S} = \frac{S}{k} = \int_{\tilde{s}_1}^{\tilde{s}_2} \tilde{\mathcal{L}}\, d\tilde{s} - \alpha\cos\psi|_{\tilde{s}_1}^{\tilde{s}_2} + \tilde{\tau}\tilde{r}_1 \tag{S.46}$$

6 Procedure for solving shape equations

We solve the shape equations in dimensionless variables, since only $\tilde{\tau}$ and $\tilde{\sigma}$ needs to be specified in this case. Note that although we work in a constant area ensemble, the membrane area is not an input to the numerical solver, but emerges from the result. The following procedure is used to obtain solutions to the shape equations (S.35)-(S.39):

1. Values for the tension parameters $\tilde{\sigma}$, $\tilde{\tau}$ are chosen along with a value of α(target) = k_G/k.
2. A point $\tilde{r}_2$, ψ_2 in the asymptotic limit is chosen ($\psi_2 \approx 0$).

3. Values of $\tilde{t}_2$ and $\dot{\tilde{\psi}}_2$ are determined from the asymptotic solution, as described above. The $\tilde{z}$-scale has an arbitrary offset and we choose $\tilde{z}_2 = 0$.
4. The shape equations (S.35)-(S.39) are integrated using the `ode45` solver in Matlab[1] with $\tilde{s}$ decreasing from 0 to $-\tilde{s}_{\text{final}}$. The value of $\tilde{s}_{\text{final}}$ is chosen sufficiently large to ensure all physical solutions are captured.
5. All solutions fulfilling equation (S.44) are stored during integration.
6. The above steps (2-5) are repeated using a 'shooting' procedure: The ratio α is determined from equation (S.43) and ψ_2 is scanned to identify the usable solutions that fulfill: $\alpha = \alpha(\text{target})$.

Note that the radius $\tilde{r}_2$ in the asymptotic limit cannot be chosen freely, but is subject to a constraint: $\tilde{r}_2 > \tilde{\tau}\tilde{\lambda}^2$. This comes from the fact that $\tilde{t}_2 > \tilde{\tau}$, i.e. integration has to start outside the edge of the hole.

Shooting is performed by varying, on a log-scale, the input angle ψ_2 in the asymptotic limit over 8 orders which is sufficient to exhaust the solution space. All solutions fulfilling the boundary in equation (S.44) are stored during integration and from these the solutions also fulfilling equation (S.43) are identified. Solutions containing self-intersecting membrane conformations are filtered out as being unphysical.
A fixed ratio of the two elastic constants $\alpha(\text{target}) = \text{k}_\text{G}/\text{k} = -0.75$ is used throughout. This value is within the span of available experimental estimates[2] and also agrees well with simulations[3].
As a reference state for the membrane energy in the curved state we use a flat membrane with the same area as the neck and without a hole.

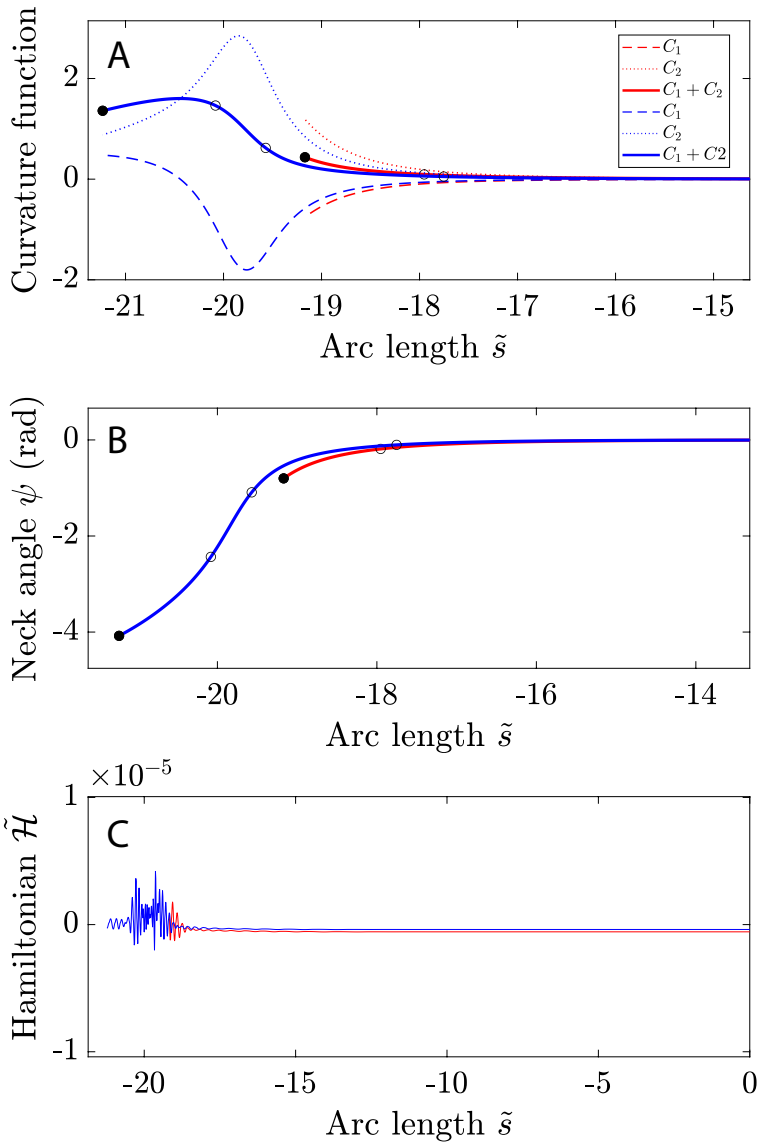

Figure S2: Plots of additional parameters related to the sample neck calculation using the line tension $\tilde{\tau}$=1 and membrane tension $\tilde{\sigma}$=-0.1. Red curves correspond to the weakly curved solution while blue correspond to the highly curved. Curvatures as function of the arc length $\tilde{s}$ are shown in (A). Here $C_1 = 1/\tilde{R}_1$ and $C_1 = 1/\tilde{R}_2$ and $C_1 + C_2$ is the total curvature in dimensionless units. The neck angle ψ is shown as function of the arc length (B). Likewise, the Hamiltonian in equation (S.41) is shown as function of the arc length.

As a control and validation of the numeric solutions, the Hamiltonian function $\tilde{\mathcal{H}}$ of equation (S.41) is plotted against the arc length $\tilde{s}$ in Figure S2C. It is found that $|\tilde{\mathcal{H}}| << 10^{-5}$ everywhere and confirming, to within the numerical precision, the prediction that $\tilde{\tilde{\mathcal{H}}}$=0, and validating the internal consistency of the shape equations (S.35-S.39). It is also found from figure S2A,S2B that the high curvature solution has a total curvature above one in the neck region and a neck angle $|\psi_1| > \pi$.

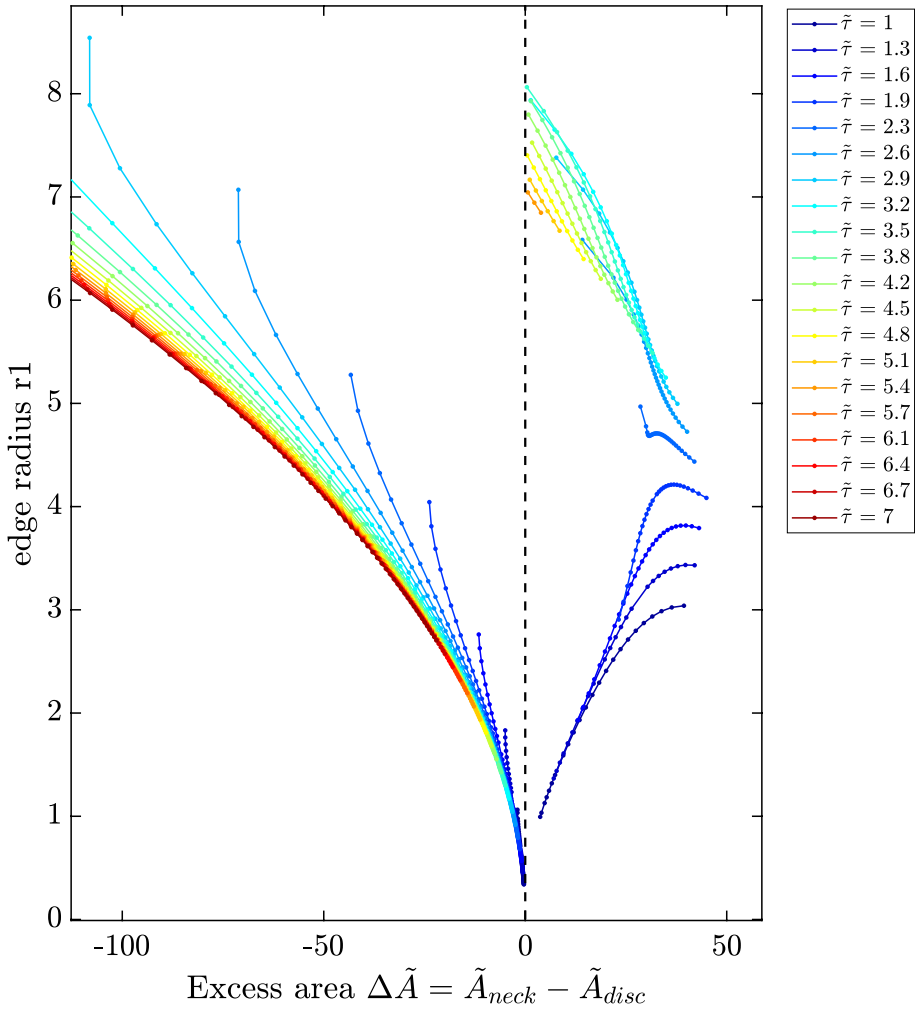

Figure S3: State diagram of the neck profiles in figure 5 in a representation of the radius r_1 of the free edge versus excess area. This figure can be compared with figure 5 which has a similar appearance, but shows the neck radius versus excess area.

References

[1] J. R. Dormand, P. J. Prince, A family of embedded Runge-Kutta formulae, Journal of computational and applied mathematics 6 (1) (1980) 19–26.

[2] D. Marsh, Handbook of lipid bilayers, CRC press, 2013.

[3] M. Hu, J. J. Briguglio, M. Deserno, Determining the Gaussian curvature modulus of lipid membranes in simulations, Biophysical journal 102 (6) (2012) 1403–1410.